Journal of Power Sources 196 (2011) 8346–8351

Contents lists available at ScienceDirect

Journal of Power Sources

journal homepage: www.elsevier.com/locate/jpowsour

Role of residual transition-metal atoms in oxygen reduction reaction in cobalt phthalocyanine-based carbon cathode catalysts for polymer electrolyte fuel cell

Masaki Kobayashi[a,b,*], Hideharu Niwa[a], Yoshihisa Harada[a,b], Koji Horiba[a,b], Masaharu Oshima[a,b], Hironori Ofuchi[c], Kiyoyuki Terakura[d], Takashi Ikeda[e], Yuka Koshigoe[f], Jun-ichi Ozaki[f], Seizo Miyata[g], Shigenori Ueda[h], Yoshiyuki Yamashita[h], Hideki Yoshikawa[h], Keisuke Kobayashi[h]

[a] Department of Applied Chemistry, School of Engineering, University of Tokyo, 7-3-1 Hongo, Bunkyo-ku, Tokyo 113-8656, Japan
[b] Synchrotron Radiation Research Organization, The University of Tokyo, 1-490-2 Kouto, Sayo-cho, Sayo-gun, Hyogo 679-5165, Japan
[c] Japan Synchrotron Radiation Research Institute (JASRI), 1-1-1 Kouto, Sayo-cho, Sayo-gun, Hyogo 679-5198, Japan
[d] Research Center for Integrated Science, Japan Advanced Institute of Science Technology (JAIST), 1-1 Asahidai, Nomi, Ishikawa 923-1292, Japan
[e] Quantum Beam Science Directorate, Japan Atomic Energy Agency (JAEA), SPring-8, 1-1-1 Kouto, Sayo-cho, Sayo-gun, Hyogo 679-5148, Japan
[f] Department of Chemical and Environmental Engineering, Graduate School of Engineering, Gunma University, 1-5-1 Tenjin-cho, Kiryu, Gunma 376-8515, Japan
[g] New Energy and Industrial Technology Development Organization, 1310 Omiya-cho, Saiwai-ku, Kawasaki, Kanagawa 212-8554, Japan
[h] NIMS Beamline Station at SPring-8, National Institute for Materials Science (NIMS), SPring-8, 1-1-1 Kouto, Sayo-cho, Sayo-gun, Hyogo 679-5148, Japan

ARTICLE INFO

Article history:
Received 17 March 2011
Received in revised form 1 June 2011
Accepted 18 June 2011
Available online 24 June 2011

Keywords:
Polymer electrolyte fuel cell
Cathode
Carbon-based catalyst
Cobalt phthalocyanine
Electronic structure
X-ray absorption fine structure

ABSTRACT

The electronic structure of Co atoms in cobalt phthalocyanine (CoPc)-based carbon catalysts, which were prepared by pyrolyzing a mixture of CoPc and phenol resin polymer up to 1000 °C, has been investigated using X-ray absorption fine structure (XAFS) analysis and hard X-ray photoemission spectroscopy (HXPES). The CoK XAFS spectra show that most of the Co atoms are in the metallic state and small quantities of oxidized Co components are present in the samples even after acid washing to remove Co atoms. Based on the difference in probing depth between XAFS and HXPES, it was found that after acid washing, the surface region with the aggregated Co clusters observed by transmission electron microscopy is primarily composed of metallic Co. Since the electrochemical properties remain almost unchanged even after the acid washing process, the residual metallic and oxidized Co atoms themselves will hardly contribute to the oxygen reduction reaction activity of the CoPc-based carbon cathode catalysts, implying that the active sites of the CoPc-based catalysts primarily consist of light elements such as C and N.

1. Introduction

Polymer electrolyte fuel cells (PEFCs) have attracted considerable attention as a clean energy source because they can operate at lower temperatures (80–100 °C) than other types of fuel cells and generate electricity through an electrochemical reaction that produces only water from hydrogen and oxygen gases. Since the reaction rate at the cathode is much lower than that at the anode, the performance of PEFCs depends on the cathode catalyst. Platinum has conventionally been employed as cathode catalyst due to its high activity for the oxygen reduction reaction (ORR) [1]. However, since Pt is precious and expensive metal, alternative materials are necessary for the realization and widespread adoption of low-cost PEFCs. There have been many reports on alternatives to Pt cathode catalysts [2], for example, Pt-*M* alloys (*M*: 3*d* transition metal), which have higher ORR activity than Pt and reduce the amount of Pt used [3–5], and pyrolyzed macrocyclic complexes such as phthalocyanine, porphyrin, and tetraazaannulene, which serve as non-noble metal catalysts [6–9].

Carbon-based catalysts are among the most promising alternatives to Pt catalysts because carbon-based catalysts are expected to be more abundant, less expensive, and more durable than Pt catalysts, due to absence of novel metal atoms [10–13]. Carbon catalysts have conventionally been synthesized by pyrolysis of organic macrocycles, carbonization of polymers containing nitrogen (and/or boron) precursors [14,15], or pyrolysis of carbon materials doped with *M*. An understanding of the active site in the carbon catalysts is essential for elucidating the mechanism of ORR and increasing ORR activity. It is considered that there are mainly three origins contributing to the ORR activity: carbon structure, impurities in carbon network, and/or active center of *M*. It has been reported that carbon structures with sp^2 hybridized orbitals such as nanotubes [10,16], nanofibers [17,18], and nanoshells [19,20], which are differentiated by the exposure of edges in graphitic

* Corresponding author at: Department of Applied Chemistry, School of Engineering, University of Tokyo, 7-3-1 Hongo, Bunkyo-ku, Tokyo 113-8656, Japan.
Tel.: +81 3 5841 7193; fax: +81 3 5841 8744.
E-mail address: mkoba@sr.t.u-tokyo.ac.jp (M. Kobayashi).

0378-7753/$ – see front matter © 2011 Elsevier B.V. All rights reserved.
doi:10.1016/j.jpowsour.2011.06.062

planes, affect the ORR activity of carbon-based catalysts. In addition, nitrogen doping improves the ORR activity of carbon catalysts [10,14], suggesting that nitrogen atoms play an important role in improving the ORR activity of the carbon catalysts [21–24]. In addition to carbon and nitrogen, the contribution of metal centers such as M–N_4 structure to the ORR activity of carbon catalysts has been investigated [25–30]. In carbon-based catalysts, the ORR active sites that determine the ORR mechanism are still in dispute.

It has been reported that M–N_x moieties including M–N_4 chelates and M–N–C complexes are possible ORR active sites in carbon catalysts [25–30], where the M atoms directly contribute to ORR activity. On the other hand, it has been hypothesized that the M atoms themselves are not active in the ORR, but rather act as a catalyst for the formation of the active sites in the carbon catalyst, as metal particles are known to be good catalysts for growth of carbon nanostructures [31–33]. M atoms in pyrolyzed carbon-based catalysts reportedly aggregate into nanoparticles covered by graphitic layers upon pyrolysis [34–36]. Therefore, understanding the detailed chemical states of the M atoms is essential for clarifying the role of M atoms in the ORR activity of carbon catalysts.

X-ray absorption fine structure (XAFS) analysis and photoemission spectroscopy (PES) are powerful tools for investigating the local geometry and electronic structure of each constituent element. In XAFS, photoabsorption from a core level to an unoccupied state occurs in an element-specific manner. The X-ray absorption signal near the absorption edge, that is, the X-ray absorption near-edge structure (XANES), reflects the electronic structure of the element. Moreover, intensity oscillation in the post-edge region as a function of photon energy, namely, the extended X-ray absorption fine structure (EXAFS), is related to the local geometry of the element (i.e., coordination number and distance to neighboring atoms) [37]. Hard X-ray photoemission spectroscopy (HXPES) enables us to investigate the element-specific electronic structure with probing depth of about10 nm from the surface [38]. In this work, we have investigated the electronic structure of Co atoms in cobalt phthalocyanine (CoPc)-based carbon catalysts, before and after acid washing, by XAFS and HXPES, where acid washing was performed to remove Co atoms. The CoPc catalysts have been prepared by pyrolysis of a mixture of CoPc and polymer and exhibit ORR activity, where the pyrolysis temperature of 1000 °C is reportedly higher than the temperatures destroying the M–N_4 structure [34]. By comparing the XAFS and HXPES spectra in this study, both the bulk and surface electronic structures of the Co clusters covered by graphitic layers of several nanometers were observed. Based on these findings, we discuss the role of Co atoms on the ORR activity.

2. Experimental

2.1. Electrochemical and structural characterization

In order to reveal the effects of M atoms on ORR activity, CoPc-based carbon catalysts were evaluated. CoPc-catalyst samples were prepared by pyrolyzing a mixture of CoPc and polymer followed by ball milling to grind the mixture. Here, planetary ball mill (Fritsch, P-7) was employed, the rotating rate was 800 rpm, and the duration was 90 min. The polymer was phenol formaldehyde resin (Gun Ei Chemical Industry Co. Ltd.). The content of Co in the precursor was adjusted to 3 wt% in the mixture of cobalt phthalocyanine and phenol resin. The mixture sat in a furnace at room temperature, and then under flowing nitrogen gas the temperature of furnace increased up to 1000 °C with a rate of 10 °C min^{-1}, and then kept at 1000 °C for 1 h. After ball milling, a portion of the pyrolyzed sample was washed with hydrochloric acid to remove Co, i.e., the samples were stirred in 12 M hydrochloric acid for 1 h, and then the samples were filtered. After this procedure, the samples were stirred again in 12 M hydrochloric acid for 12 h. Hereinafter, the CoPc-based catalysts (CoPc-PhRs1000) before and after acid washing are referred to as the "as-grown" and "acid-washed" samples, respectively.

Transmission electron microscopy (TEM) observation of the acid-washed sample was performed by placing the sample on a grid that was coated with a carbon film. The transmission electron microscope (JEM2010, JEOL) was operated at an acceleration voltage of 200 keV. The ORR activity was evaluated by rotating ring disk electrode (RRDE) voltammetry in 0.5 mol L^{-1} H_2SO_4 saturated with oxygen at room temperature. Conditions of the RRDE measurements were as follows: rotation rate – 1500 rpm, potential scan rate – 1 mV s^{-1}, and catalyst loading density – 0.20 mg cm^{-2}. The electrolyte was nitrogen saturated 0.5 M H_2SO_4. The scanning range was from 0.8 to −0.2 V vs. Ag/AgCl with the scanning rate of 50 mV s^{-1} and the cycle number of 5 times. In this work, the oxygen reduction potential E_{O_2} is defined as the voltage at which a reduction current density of −10 μA cm^{-2} is reached.

2.2. X-ray absorption and photoemission spectroscopy measurements

XAFS measurements were performed at beamline BL14B2 of SPring-8 with a Si(1 1 1) double crystal monochromator. The XAFS spectra of the samples and references were measured in the fluorescence-detection and transmission modes at room temperature, respectively. The X-ray fluorescence signals were detected by an array of 19-element Ge solid-state detectors. The monochromator resolution was $E/\Delta E > 10{,}000$. The analysis of the EXAFS data was performed with the REX2000 program produced by Rigaku Ltd. [39]. Curve fitting for the EXAFS spectra was performed by *ARTEMIS* software [40] and FEFF6L [41]. HXPES measurements were performed at the hard X-ray beamline BL15XU of SPring-8 at room temperature. The incident photon energy was 5.95 keV. The base pressure was approximately 3×10^{-7} Pa. The total resolution of the HXPES measurements including temperature broadening was about 200 meV. The Fermi energy (E_F) was determined by measuring the PES spectra of evaporated gold that was electrically in contact with the surface of the samples. Co-metal foil and CoPc were also measured by HXPES as reference.

3. Results and discussion

3.1. Transmission electron microscopy

Fig. 1 shows a TEM image of the acid-washed CoPc-PhRs1000 sample. The image indicates that aggregated clusters remain in the CoPc-PhRs1000 even after acid washing to remove the Co atoms. It can also be seen that the sample has shell-like carbon structures, as in the cases of ferrocene-poly(furfuyl alcohol) mixture [19] and Co-[poly(4-vinylpyridine)] complex [20]. The shell-like structures originate from graphitic multilayers, which are thought to be related to ORR activity [20]. The average diameters of the Co clusters and carbon shells are 8 nm and 20 nm, respectively.

3.2. RRDE voltammetry

Table 1 lists the electrochemical properties of the samples. E_{O_2} reflects the ORR activity of the catalysts. The voltammograms of the samples have been shown as Fig. 1 in Ref. [42]. Comparing the samples before and after the acid washing, E_{O_2} of the as-grown sample was found to be the same as that of the acid-washed sample although about 40% of total amount of Co was removed by the acid washing [42]. On the other hand, the current density $i_{0.7}$ increases upon acid washing. These results suggest that the acid washing does not affect the density of active sites but improves the conductivity of the sample, as in the case of washing pyrolyzed acetonitrile with

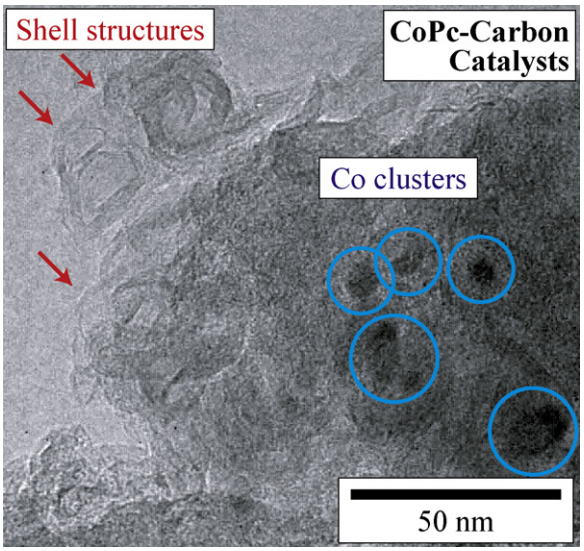

Fig. 1. Transmission electron microscopy image of acid-washed CoPc-PhRs1000 catalyst. Arrows and circles denote shell-like carbon structures and Co clusters, respectively.

HF over alumina impregnated with Fe or Ni [17]. It should be noted that the current density of the present CoPc-based carbon catalysts is improved after the acid washing.

3.3. Co K XAFS

3.3.1. XANES

In order to investigate the electronic structure of the Co atoms, the XANES spectra of the CoPc-PhRs1000 samples were compared with those of several Co species, as shown in Fig. 2(a). Here, the XANES spectra of the samples are normalized to the post-edge area. It appears that the peaks at 7714 eV, 7729 eV, and 7738 eV are characteristic for hcp Co metal (Co^{0+} D_h), fcc Co metal (Co^{0+} O_h) [43], Co carbide (Co–C) [44], CoO (Co^{2+} O_h), and CoPc (Co^{2+} D_{4h}), respectively. After acid washing, relatively, the intensity of the peak at 7714 eV slightly increases, while the intensity of the peak at 7729 eV decreases. This result suggests that the electronic structure of Co changes upon acid washing. In order to quantitatively estimate the relative amounts of Co components present in the catalyst, the Co *K* XANES spectra are reproduced by combining possible Co components, namely, hcp Co metal (Co^{0+} D_h), fcc Co metal (Co^{0+} O_h) [43], Co carbide (Co–C) [44], CoPc (Co^{2+} D_{4h}), Co_3O_4 (Co^{2+} T_d and Co^{3+} O_h), CoO (Co^{2+} O_h), and $LaCoO_3$ (Co^{3+} O_h). The results are listed in Table 2 and shown in Fig. 2. Although the fitted curves reproduce most of the peak structures, there are some differences between the experimental data and fitted curves, as shown in Fig. 2(a) and (b), implying that small amounts of other Co oxides might be present in the samples.

3.3.2. EXAFS

Fig. 3(a) shows k^3-weighted EXAFS oscillation of the CoPc-PhRs1000 catalysts. As shown in Fig. 3(b) and (c), the Fourier transform of the k^3-weighted EXAFS oscillation of samples has similar line shape and shows a peak around approximately 2.15 Å, which is similar to pure Co metal. The Fourier-transformed oscillation of the samples has low intensity at the peak positions of the CoPc and CoO spectra, indicating that there are few CoPc and CoO-like components in the samples, which is consistent with the results of the decomposition analysis of the XANES spectra. The intensity at approximately 2.15 ± 0.01 Å is lower than that of Co metal, as shown in Fig. 3(b) and (c). In fact, the curve fitting reveals that the coordination number (N) of 8.0 ± 0.4 and 8.5 ± 0.4 of the Co–Co component for the as-grown and acid-washed samples, respectively, is smaller than that of bulk Co metal ($N_{\text{Co-metal}} = 12$). The atomic distance R between the Co ion and nearest neighbors and the coordination number N of the Co ion have been estimated from the EXAFS spectra and the values are listed in Table 3. Comparing samples before and after acid washing, the estimated distance to the neighboring Co remains almost unchanged, while the obtained coordination number N is different between the as-grown and acid-washed samples. We cannot adequately discuss the origin of the difference in the coordination number due to large error bars.[1]

3.3.3. Residual Co components

Let us summarize information obtained by the XANES and EXAFS analyses to evaluate the Co components before and after acid washing. In both the as-grown and acid-washed samples, most of the Co atoms are in the metallic state (Co^{0+} D_h, Co^{0+} O_h, and Co–C) and there is a small amount of the Co^{2+} D_{4h} component, indicating that the thermal procedure during the preparation of the samples chemically converts most of the Co ions of CoPc into metallic Co. The result that the metallic Co components are dominant in the samples is likely consistent with the previous report that pyrolysis temperature higher than 700 °C destroys the Co-N_4 structure in CoPc-based catalysts and leads to appearance of metallic Co particles [34]. A small amount of the Co^{2+} O_h component is present in the sample, and the signal from the Co^{3+} O_h and Co^{2+} + Co^{3+} components are undetectable. Note that acid washing decreases the Co^{2+} O_h components relative to the metallic component, implying that the Co^{2+} O_h component is more removed than the metallic Co by the acid washing.

The lower coordination number N than the metallic cobalt could be affected by the clustering of cobalt. The relative amount of the metallic Co component compared with the total amount of Co atoms ($r_{\text{Co-metal}}$) is 0.869 (86.9%)[2] and the average diameter of the aggregated Co cluster is approximately 8 nm. For an fcc Co-metal cluster with a diameter of 8 nm, the ratio r_{surf} between the number of surface atoms and the total number of atoms is 0.091 (9.1%).[3] For the fcc structure, the surface atoms have an approximate coordination number N_{surf} of 7.3 ($N = 8$ for the (1 0 0) plane surface, and $N = 7$ for the (1 1 0) and (1 1 1) plane surfaces). Then assuming that the Co clusters only consist of metallic Co and the lattice constant of

Table 1
Electrochemical activity for oxygen reduction reaction of CoPc-PhRs1000 catalysts measured by rotating disk electrode voltammetry. Oxygen reduction potential E_{O_2} is defined as the voltage at which reduction current density of -10 μA cm^{-2} is reached. Current density at 0.70 V vs. NHE ($i_{0.7}$) is also listed.

	E_{O_2} (V vs. NHE)	$i_{0.7}$ (μA cm^{-2})
As-grown	0.75	−46.4
Acid-washed	0.75	−49.8

[1] Since the distinction between the light elements (C, N, and O) is probably difficult in the EXAFS analysis (for example, distance of Co–N bond in CoPc of 1.9 Å is close to that of Co–C one in Co_3C of 1.9 Å), the two bonds have been employed for fitting, i.e., Co–Co and Co–C bonds. Here, the Co–C bond represents bonds between Co and the light elements.

[2] The amount is based on the amount of Co-metal (hcp and fcc) and Co–C components estimated from the decomposition analysis. Here, the Co–C component is assumed to be Co_3C. Therefore, total amount of the Co-metal and 75% of the Co–C is the amount of metallic Co. The value is averaged between the as-grown and acid-washed samples.

[3] Surface volume of a cluster is assumed to be hollow sphere having thickness of lattice constant (the diameter is the same as the cluster). The number of surface atoms is estimated from dividing the volume of hollow sphere by the volume per an atom. When the diameter of cluster increases, the ratio between the number of surface atoms and the total number of atoms decreases because the thickness of hollow sphere is fixed as the lattice constant.

Table 2
Results of decomposition analysis of Co *K* XANES spectra of CoPc-PhRs1000 catalysts. Error bars represent ±3.0%.

	Co^{0+} D_h	Co^{0+} O_h	Co–C	Co^{2+} D_h	Co^{2+} + Co^{3+}	Co^{2+} O_h	Co^{3+} O_h
As-grown	43.6%	33.1%	10.6%	3.7%	0%	4.5%	4.5%
Acid-washed	47.0%	37.7%	5.8%	5.0%	0%	0.2%	4.3%

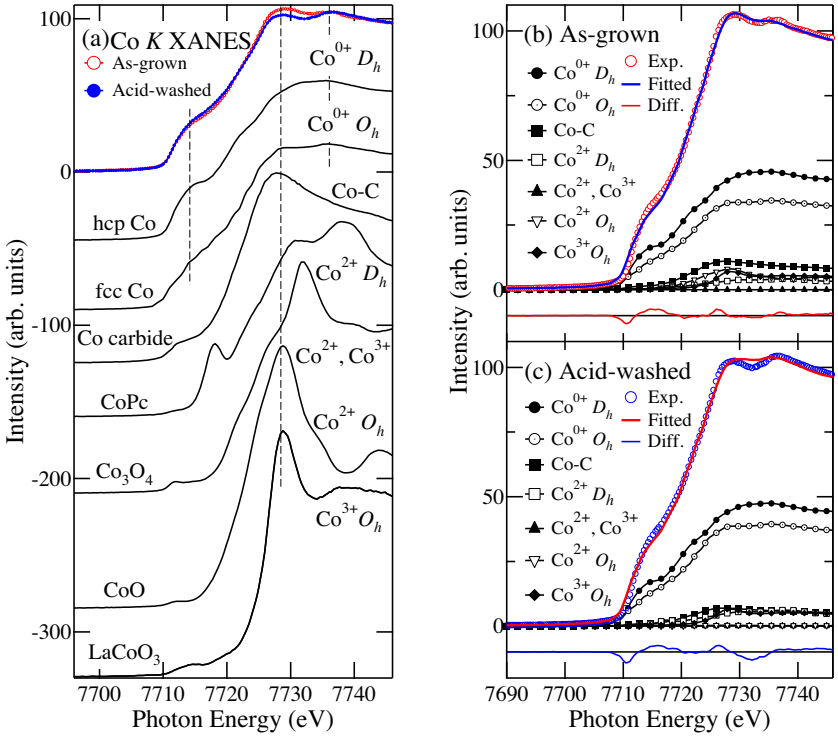

Fig. 2. Co *K* XANES spectra of CoPc-PhRs1000 catalysts. (a) Comparison between Co *K* XANES spectra of Co compounds. References are hcp Co metal (Co^{0+} D_h), fcc Co metal (Co^{0+} O_h) [43], Co carbide (Co–C) [44], CoPc (Co^{2+} D_{4h}), Co_3O_4 (Co^{2+}, Co^{3+}: Co^{2+} O_h, Co^{3+} T_d, and Co^{3+} T_d), CoO (Co^{2+} O_h), and $LaCoO_3$ (Co^{3+} O_h). Dashed lines are guides for the eye. (b and c) Decomposition analysis of spectra of the as-grown and acid-washed CoPc-carbon catalysts, respectively. Difference between the experiment spectra and the results of fitting are also shown, and the offsets for the difference spectra are −10.

Table 3
Results of curve fitting for the Fourier-transformed EXAFS oscillation $k^3\chi$ of the CoPc-PhRs1000 catalysts. The atomic distance *R* (Å), coordination number *N*, Debye–Waller factor σ^2 (Å^2), and energy shift ΔE_0 (eV) are listed. The values in blankets denote error bar.

	Bond type	*R* (Å)	*N*	σ^2 (Å^2)	ΔE_0 (eV)
As-grown	Co–Co	2.495 (0.002)	8.0 (0.4)	0.0057 (0.003)	−0.22 (0.48)
	Co–C	2.062 (0.042)	1.3 (0.2)	0.0128 (0.0143)	−0.22 (0.48)
Acid-washed	Co–Co	2.491 (0.002)	8.5 (0.4)	0.0057 (0.003)	−0.87 (0.42)
	Co–C	2.085 (0.042)	0.9 (1.4)	0.0154 (0.0304)	−0.87 (0.42)

hcp Co is approximately the same as fcc Co (the number of nearest neighbors of hcp Co is the same as fcc Co and the volume per atom of 11.09 Å^3 in hcp Co is almost the same as that of 11.14 Å^3 in hcp Co [45]), the average coordination number of the Co–Co components N_{calc} can be calculated:

$$N_{calc} = r_{Co\text{-}metal} \times [N_{surf} \times r_{surf} + N_{Co\text{-}metal} \times (1 - r_{surf})] = 10.1 \quad (1)$$

This estimated value of N_{calc} is slightly larger than the coordination number *N* of 8.0 or 8.5 ± 0.4 estimated from the EXAFS analysis (79.2 or 84.2 ± 4.0% of the N_{calc} for the Co-metal cluster), suggesting that the Co clusters are primarily composed of metallic Co and may include a small amount of oxidized Co components and/or a porous structure (the total amount of about 15%).

3.4. HXPES

The probing depth of Co 2*p* HXPES of about 10 nm is shorter than that of Co *K* XAFS that probes several micrometers. Since the Co clusters are covered by shell structures having a thickness of about 10 nm, the surface and bulk electronic structures of the Co clusters can be evaluated by taking advantage of this difference in probing depth. In addition to the surface of Co clusters, HXPES also probes the surface of the pores/channels inside the catalysts. Fig. 4 shows the Co 2*p* HXPES spectra of the CoPc-PhRs1000 catalysts. The intensities are normalized to the total number of incident photons. There are two characteristic peaks in the as-grown sample. The sharp and broad peaks at 778 eV and 781 eV are assigned to metallic Co (Co^{0+}) and oxidized Co (Co^{2+}) components, respectively [46]. It is probable that the oxidized Co states of the as-grown sample predominantly originate from the CoPc- and CoO-like components observed by XANES. In the as-grown sample, the Co 2*p* HXPES intensity of the metallic Co state is almost the same as that of the oxidized Co states, while the metallic Co component observed by the Co *K* XANES is much larger than the oxidized Co component. These observations indicate that the oxidized Co ions coexist with the metallic Co atoms at the surface of the Co clus-

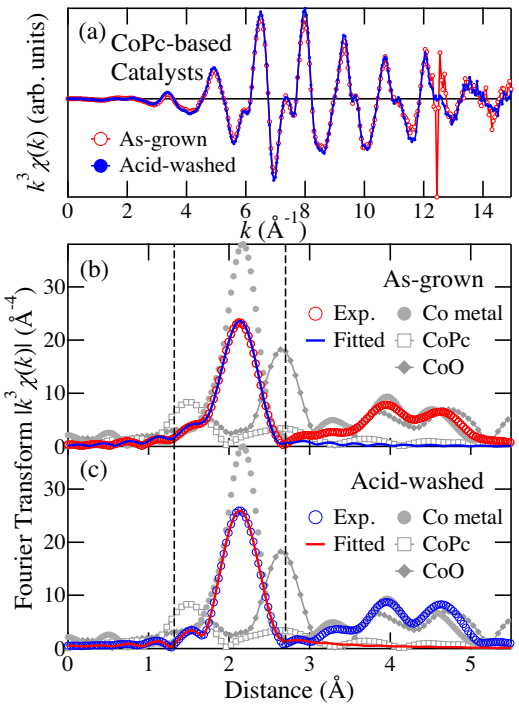

Fig. 3. Co *K* EXAFS spectra of CoPc-PhRs1000 catalysts. (a) k^3-Weighted EXAFS oscillations. Fourier transform of the k^3-weighted EXAFS oscillation as a function of atomic distance for (b) as-grown and (c) acid-washed samples and the fitted spectra are shown. Here, ranges between the vertical dashed lines correspond to the fitting range. The spectra of Co metal, CoO, and CoPc are also plotted as reference.

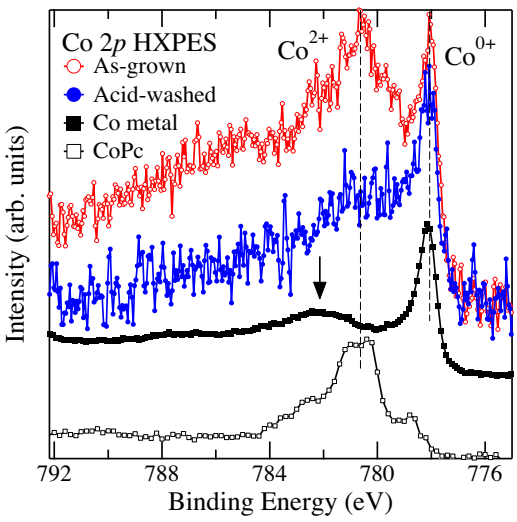

Fig. 4. Co 2*p* HXPES spectra of CoPc-PhRs1000 catalysts. Constant values have been subtracted from spectra corresponding to the height on the lower binding energy side of the main peak. The intensities are normalized to total photon flux in order to enable comparison of Co contents between the two samples. Dashed lines are guides for the eye. As reference, Co 2*p* HXPES spectra of Co metal and CoPc are also shown. The arrow denotes oxidized Co components on the surface of Co metal.

ters or pores/channels inside the catalysts in the as-grown sample. In contrast, in the acid-washed sample, the signal from the oxidized Co components is hardly detectable and a slight decrease in the signal of the metallic Co component compared with that of the as-grown sample is observed. This result suggests that the acid washing process removes a portion of the metallic Co and most of the oxidized Co ions from the surface of aggregated Co clusters of the surface of the pores/channels inside the catalysts. In contrast, the electronic structures of C and N were nearly unchanged by the acid-washing [42]. It should be noted that although the oxidized Co components are detected by XAFS, the surface of Co clusters are primarily composed of the metallic Co component after acid washing.

3.5. Discussion

Finally, we discuss the relationship between the ORR catalytic properties and the role of Co atoms, based on the experimental findings. Comparing the electrochemical properties of the as-grown and acid-washed samples, the electrochemical properties are slightly improved by acid washing, as described above (see Table 1), which suggests that the Co components removed by acid washing hardly contribute to the improvement of ORR activity. The metallic and oxidized Co components observed by HXPES are reduced by acid washing, and it is likely that these components are not responsible for the ORR activity of the CoPc-PhRs1000 catalysts. The result that residual Co metal is inactive for ORR is consistent with reports on the rotating disk voltammetry of pure Co metal [4] and Co metal supported by carbon (Co loading of 1.2%) [11]. It follows from these arguments that Co atoms which mainly consist of metallic and oxidized Co components do not significantly make a direct contribution to the ORR activity of the CoPc-PhRs1000. It is also worth noting that the Co nanoclusters predominantly consist of metallic Co components. It has been reported that metal nanoparticles such as Fe and Co act as catalysts for the growth of carbon nanotubes [47], and the nanoparticles are encapsulated by graphitic multilayers upon pyrolysis at temperatures lower than those required to grow carbon nanotubes [48]. In regards to the encapsulation, it has been reported that metal nanoparticles with diameter less than 2 nm are not encapsulated [49] and that the number of encapsulating graphitic layers increases with increasing diameter of the metal nanoparticles [50,51]. The result that the nanoshell structures had 20 nm (8 graphitic layers) on average, as estimated from TEM images, is similar to the report on the encapsulation of 7-nm particles by 6 graphitic layers [52]. Therefore, we conclude that the metallization of Co is related to development of the carbon nanoshell structure in the CoPc-based carbon catalysts.

4. Conclusion

In conclusion, we have performed XAFS and HXPES measurements on CoPc-based catalysts, which were pyrolyzed up to 1000 °C, before and after acid washing in order to investigate the relationship between ORR activity and the presence of Co atoms. The decomposition analysis of the Co *K* XANES spectra demonstrated that the Co clusters are predominantly composed of metallic Co with only small quantities of oxidized components. The analysis for the EXAFS spectra suggested that the aggregated Co clusters in the CoPc-PhRs1000 catalysts that were observed by TEM are mainly composed of metallic Co. Acid washing effectively reduced the total amount of Co, and the oxidized Co components on the surface of the Co clusters were preferentially removed. Comparing the above results with the electrochemical properties before and after acid washing, we conclude that both the metallic and oxidized Co components are inactive for the ORR in the CoPc-PhRs1000 catalysts. It follows from these arguments that the residual Co atoms themselves are not ORR active site in the CoPc-based carbon catalysts pyrolyzed at high temperatures, implying that the active sites of the CoPc-based carbon catalysts should reside on light elements such as C and N.

Acknowledgments

This work was performed under Project 08003440-0 at the New Energy and Industrial Technology Development Organization (NEDO). XAFS experiments at SPring-8 were approved by the Japan Synchrotron Radiation Research Institute (JASRI) Proposal Review Committee (Proposal No. 2008B2167). HXPES measurements were performed under the approval of the NIMS Beamline Station (Proposal No. 2008A4801). The authors are grateful to HiSOR, Hiroshima University and JAEA/SPring-8 for the development of HXPES at beamline BL15XU of SPring-8.

References

[1] X. Yu, S. Ye, J. Power Sources 172 (2007) 145–154.
[2] B. Wang, J. Power Sources 152 (2005) 1–15.
[3] S. Mukerjee, S. Srinvasan, J. Electroanal. Chem. 357 (1993) 201–224.
[4] T. Toda, H. Igarashi, H. Uchida, M. Watanabe, J. Electrochem. Soc. 146 (1999) 3750–3756.
[5] V.R. Stamenkovic, B.S. Mun, M. Arenz, K.J.J. Mayrhofer, C.A. Lucas, G. Wang, P.N. Ross, N.M. Markovic, Nat. Mater. 6 (2007) 241–247.
[6] M. Bron, J. Radnik, M. Fieber-Erdmann, P. Bogdanoff, S. Fiechter, J. Electroanal. Chem. 535 (2002) 113–119.
[7] X. Deng, X. Wang, Z.-F. Ma, J. Power Sources 183 (2008) 604–608.
[8] H.-J. Zhang, X. Yuan, W. Wen, D.-Y. Zhang, L. Sun, Q.-Z. Jiang, Z.-F. Ma, Electrochem. Commun. 11 (2008) 206–208.
[9] C.W.B. Bezerra, L. Zhang, K. Lee, H. Liu, A.L.B. Marques, E.P. Marques, H. Wang, J. Zhang, Electrochim. Acta 53 (2008) 4937–4951.
[10] K. Gong, D. Du, Z. Xia, M. Durstock, L. Dai, Science 323 (2009) 760–764.
[11] R. Bashyam, P.A. Zelenay, Nature 443 (2006) 63–66.
[12] B. Winther-Jensen, O. Winther-Jensen, M. Forsyth, D.R. MacFarlane, Science 321 (2008) 671–674.
[13] E.J. Biddinger, D. von Deak, U.S. Ozkan, Top. Catal. 52 (2009) 1566–1574.
[14] J. Ozaki, N. Kimura, T. Anahara, A. Oya, Carbon 45 (2007) 1847–1853.
[15] J. Ozaki, T. Anahara, N. Kimura, A. Oya, Carbon 44 (2006) 3358–3361.
[16] M. Gao, S. Huang, L. Dai, G. Wallace, R. Gao, Z. Wang, Angew. Chem., Int. Ed. Engl. 39 (2000) 3664–3667.
[17] P.H. Matter, E. Wang, M. Arias, E.J. Biddinger, U.S. Ozkan, J. Phys. Chem. B 110 (2006) 18374–18384.
[18] P.H. Matter, E. Wang, J.-M. Millet, U.S. Ozkan, J. Phys. Chem. C 111 (2007) 1444–1450.
[19] J. Ozaki, K. Nozawa, K. Yamada, Y. Uchiyama, Y. Yoshimoto, A. Furuichi, T. Yokoyama, A. Oya, L.J. Brown, J.D. Cashion, J. Appl. Electrochem. 36 (2006) 239–247.
[20] R. Kobayashi, J. Ozaki, Chem. Lett. 38 (2009) 396–397.
[21] P.H. Matter, L. Zhang, U.S. Ozkan, J. Catal. 239 (2006) 83–96.
[22] T. Ikeda, M. Boero, S.-F. Huang, K. Terakura, M. Oshima, J. Ozaki, J. Phys. Chem. C 112 (2008) 14706–14709.
[23] H. Niwa, K. Horiba, Y. Harada, M. Oshima, T. Ikeda, K. Terakura, J. Ozaki, S. Miyata, J. Power Sources 187 (2009) 93–97.
[24] Y. Shao, J. Sui, G. Yin, Y. Gao, Appl. Catal. B: Environ. 79 (2008) 89–99.
[25] G. Faubert, G. Lalande, R. Cote, J.-P. Dodelet, L.T. Weng, P. Bertrand, G. Denes, Electrochim. Acta 41 (1996) 1689–1701.
[26] M. Yuasa, A. Yamaguchi, H. Itsuki, K. Tanaka, M. Yamamoto, K. Oyaizu, Chem. Mater. 17 (2005) 4278–4281.
[27] H. Tributsch, U.I. Koslowski, I. Dorbandt, Electrochim. Acta 53 (2008) 2198–2209.
[28] M. Lefèvre, E. Proietti, F. Jaouen, J.-P. Dodelet, Science 324 (2009) 71–74.
[29] A.B. Anderson, R.A. Sidik, J. Phys. Chem. B 108 (2004) 5031–5035.
[30] U.I. Koslowski, I. Abs-Wurmbach, S. Fiechter, P. Bogdanoff, J. Phys. Chem. C 112 (2008) 15356–15366.
[31] N.M. Rodriguez, A. Chambers, R.T.K. Baker, Langmuir 11 (1995) 3862–3866.
[32] S. Hofmann, R. Blume, C.T. Wirth, M. Cantoro, R. Sharma, C. Ducati, M. Havecker, S. Zafeiratos, P. Schnoerch, A. Oestereich, D. Teschner, M. Albrecht, A. Knop-Gericke, R. Schlogl, J. Phys. Chem. C 113 (2009) 1648–1656.
[33] N. Li, X. Wang, F. Ren, G.L. Haller, L.D. Pfefferle, J. Phys. Chem. C 113 (2009) 10070–10078.
[34] M.C. Martins Alves, J.P. Dodelet, D. Guay, M. Ladouceur, G. Tourillon, J. Phys. Chem. 96 (1992) 10898–10905.
[35] M. Ladouceur, G. Lalande, D. Guay, J.-P. Dodelet, L. Dignard-Bailey, M.L. Trudeau, R. Schulz, J. Electrochem. Soc. 140 (1993) 1974–1981.
[36] L.T. Weng, P. Bertrand, G. Lalande, D. Guay, J.-P. Dodelet, Appl. Surf. Sci. 84 (1995) 9–21.
[37] J.J. Rehr, R.C. Albers, Rev. Mod. Phys. 72 (2000) 621–654.
[38] Y. Takata, K. Tamasaku, T. Tokushima, D. Miwa, S. Shin, T. Ishikawa, M. Yabashi, K. Kobayashi, J.J. Kim, T. Yao, T. Yamamoto, M. Arita, H. Namatame, M. Taniguchi, Appl. Phys. Lett. 84 (2004) 4310–4312.
[39] T. Taguchi, T. Ozawa, H. Yahiro, Phys. Scripta T105 (2005) 205–206.
[40] B. Ravel, M. Newville, J. Synchrotron Radiat. 12 (2005) 537–541.
[41] J.J. Rehr, S.I. Zabinsky, R.C. Albers, Phys. Rev. Lett. 69 (1992) 3397.
[42] H. Niwa, M. Kobayashi, K. Horiba, Y. Harada, M. Oshima, K. Terakura, T. Ikeda, Y. Koshigoe, J. Ozaki, S. Miyata, S. Ueda, Y. Yamashita, H. Yoshikawa, K. Kobayashi, J. Power Sources 196 (2011) 1006–1011.
[43] R. Torchio, C. Meneghini, S. Mobilio, G. Capellini, A. García Prieto, J. Alonso, M.L. Fdez-Gubieda, V. Turco Liveri, A. Longo, A.M. Ruggirello, T. Neisius, J. Phys.: Conf. Ser. 200 (2010) 072100.
[44] B. Jiang, D.-S. Yang, A.N. Ulyanov, S.-C. Yu, J. Appl. Phys. 95 (2004) 7115–7117.
[45] G.Y. Guo, H.H. Wang, Chin. J. Phys. 38 (2000) 949.
[46] C.D. Wagner, W.M. Riggs, L.E. Davis, J.F. Moulder, in: G.E. Muilenberg (Ed.), Handbook of X-ray Photoelectron Spectroscopy, Perkin-Elmer, Minnesota, 1979.
[47] Y. Homma, Y. Kobayashi, T. Ogino, D. Takagi, R. Ito, Y.J. Jung, P.M. Ajayan, J. Phys. Chem. B 107 (2003) 12161–12164.
[48] N. Sano, H. Akazawa, T. Kikuchi, T. Kanki, Carbon 41 (2003) 2159–2179.
[49] J.H. Hafner, M.J. Bronikowski, B.R. Azamian, P. Nikolaev, A.G. Rinzler, D.T. Colbert, K.A. Smith, R.E. Smalley, Chem. Phys. Lett. 296 (1998) 195–202.
[50] J. Gavillet, J. Thibault, O. Stephan, H. Amara, A. Loiseau, C. Bishara, J.-P. Gaspard, J. Ducastelle, J. Nanosci. Nanotechnol. 4 (2004) 346–359.
[51] F. Ding, A. Rosen, E.E.B. Campbell, L.K.L. Falk, K. Bolton, J. Phys. Chem. B 110 (2006) 7666–7670.
[52] K. Bladh, L.K.L. Falk, F. Rohmund, Appl. Phys. A 70 (2000) 317–322.